Structure sensitivity of electrochemical adsorption and reduction of acetol on noble metal electrodes

Liang, Z.; Villalba, M.A.; Koper. M.T.M.

Electrochimica Acta 391 (2021) 138911

Contents lists available at ScienceDirect

Electrochimica Acta

journal homepage: www.elsevier.com/locate/electacta

Structure sensitivity of electrochemical adsorption and reduction of acetol on noble metal electrodes

Zhiqin Liang, Matias A. Villalba, Marc T.M. Koper*

Leiden Institute of Chemistry, Leiden University, PO Box 9502, 2300 RA Leiden, the Netherlands

ARTICLE INFO

Article history:
Received 8 May 2021
Revised 21 June 2021
Accepted 8 July 2021
Available online 17 July 2021

ABSTRACT

Acetol – a dehydration product of glycerol – can be selectively reduced to 1,2-propanediol and acetone through hydrogenation and dehydroxylation reactions, thereby providing a platform toward an efficient upgrading of biomolecules. To shed light on the relationship between the reactivity and the electrode structure, we report the electrochemical reduction of acetol on low-index platinum single crystals and their corresponding epitaxial palladium monolayers (Pd_{ML}). Combining cyclic voltammetry and *in-situ* spectroscopy measurements, Pt(110) and Pt(111) are shown to be active surfaces for acetol adsorption and reduction at potentials near 0 V vs.RHE, though accompanied by the dissociative adsorption of acetol to poisoning CO. For the Pt(100) surface, the activities of both acetol reduction and hydrogen evolution are inhibited by the most prominent CO poisoning among the three surfaces. In contrast, no electrochemical acetol reduction is detected on palladium monolayer near 0 V vs.RHE, irrespective of the surface crystallographic orientation. However, acetol decarbonylation still proceeds especially on $Pd_{ML}Pt(110)$, which suffers from the most severe poisoning from the low-index surfaces. Furthermore, to access practical applications, we extend the study on the effect of the electrode material, the applied potential, and the electrolyte pH on the selectivity of acetol reduction. At sufficiently negative potentials, Au and Pt are appropriate candidates toward hydrogenation reaction to 1,2-propanediol at Ph = 3, whereas Pd exhibits the ability to produce both 1,2-propanediol and acetone at pH = 1 and pH = 3, the selectivity of which is strongly dependent on the potential. Given these mechanistic insights into acetol adsorption and reduction at the specific electrodes and facets, this work provides guidance on how to rationally design electrocatalysts toward efficient electrochemical hydrogenation.

1. Introduction

Electrochemical conversion of biomass feedstock to value-added chemicals and fuels would be a significant step toward a carbon-neutral cycle, allowing for an upgrading platform using renewable electricity [1–3]. On the one hand, biomass originating from the decomposition of lignocellulose through pyrolysis or hydrolysis processes results in a complex mixture of acids, alcohols, and ketones [4]. The further refinery of these compounds is of paramount importance to produce useful intermediates or potential transportation fuels. On the other hand, compared to conventional petrochemical-derived processes, which run at high temperature and pressure, as well as using hydrogen as the reducing agent [5], electrocatalytic routes have emerged as a promising alternative which may be more environment-friendly and may offer better safety.

Studies on electrochemical hydrogenation of carbonyl compounds, such as 5-hydroxymethylfurfural [6], glucose [7], ethyl pyruvate [8], have therefore attracted great attention. Since they involve multiple functional groups, the active and selective conversion of these molecules are correlated closely with the electrode surface and the chemical environment [9]. To design a catalyst toward an efficient electrochemical process, it is important to build a structure – reactivity relationship to understand the interaction between the surface and the molecules. However, for most catalysts, it is difficult to isolate the surface structure effects from other variables, such as structural heterogeneity, multiple defects, and support interactions [8].

Well-ordered single crystals offer a platform to deconvolute such effects, which in turn may guide the rational design of electrocatalysts with the desired structure. For example, acetone, as the simplest ketone, has been investigated as a model reaction on platinum (Pt) single crystals [10]. It was found that acetone reduction is highly structure sensitive: on surfaces with a (111) terrace and (110) steps, it is hydrogenated to 2-propanol, while on surfaces

* Corresponding author.
E-mail address: m.koper@chem.leidenuniv.nl (M.T.M. Koper).

https://doi.org/10.1016/j.electacta.2021.138911

with a (100) terrace and (110) steps, the hydrogenolysis product, i.e. propane, is produced. This trend was also observed for longer aliphatic ketones.

The reactivity of ketones is influenced by their further chemical functionalization, which might modify the adsorption energies or the spatial configuration of these functional groups on the electrode surface. Taking the same example of acetone reduction, the adsorption of acetone is unfavorable at the (111) and (100) facets of the Pt surface, thus no reduction proceeds [10]. However, functionalization of acetone with a phenyl ring to acetophenone makes the molecule bind on the Pt surface through π-electron system [11–13]. As a result, acetophenone activation is enabled, facilitating hydrogenation of the carbonyl group to 1-pheylethanol on Pt(111) and hydrogenolysis to ethylbenzene on the Pt(100) surface [14].

In addition to platinum, palladium (Pd) electrodes have also been widely used for electrochemical hydrogenation reactions [15, 16], showing significantly higher activity than Pt in certain cases [17]. As the Pd bulk material absorbs hydrogen into the lattice below 0.2 V vs.RHE, the reduction current is dominated by hydrogen formation, making it difficult to understand the relationship between electrode structure and reactivity for electrochemical hydrogenation. Our group has previously used Pd monolayer deposition on the Pt surface by epitaxial growth, to investigate the electrochemical hydrogenation of acetophenone. It has been pointed out that bulk Pd electrode and Pd monolayer on Pt electrode have similar electronic properties, as well as that the Pd monolayer surface keeps the atomic arrangement of the Pt substrate, mimicking the surface Pd orientation. [18]

In light of the aforementioned fundamental understanding of the electrode activity, we return to organic electrosynthesis for biomass upgrading. In previous work, we have demonstrated the reduction of glyceraldehyde (GA) and dihydroxyacetone (DHA) – intermediates arising from the selective glycerol oxidation [19–21] – to a series of products with higher value or larger market size, such as 1,3-propanediol (1,3-PD) or acetone [22]. In this paper, we continue to pursue a cascade upgrading from glycerol as it is challenging to reduce glycerol directly due to the negative reduction potential of their hydroxyl groups [23].

Our strategy here is to start with hydroxyacetone (acetol), which we observed as one of the products of dihydroxyacetone reduction [22], (which has also been achieved by a non-electrochemical dehydration of glycerol with selectivity higher than 90% [24,25]). Acetol can then be followed by a second electrocatalytic hydrogenation/dehydroxylation to 1,2-propanediol (1,2-PD) or acetone [26].

To this end, we employ single-crystal Pt and Pd monolayer on Pt electrode to study the fundamentals of acetol adsorption and reduction. Knowing the activity on different facets, we then extend the study to other electrodes, different electrolyte pH, and more negative potentials, to show the selective reduction of acetol to 1,2-PD and acetone, respectively. In this way, we can identify the catalysts and reaction conditions needed in the cascade upgrading of glycerol to 1,3- and 1,2-PD.

2. Experimental section

Chemicals and Electrolysis. The chemicals used for electrolyte preparation were high-purity sulfuric acid (H_2SO_4, Merck Suprapur, 96%), hydrochloride acid (HCl, Merck Suprapur, 37%), and sodium sulfate (Na_2SO_4, Sigma-Aldrich, >99%). Palladium sulfate ($PdSO_4$, 99%), palladium chloride ($PdCl_2$, 99.99%), and acetol (95%) were purchased from Alfa Aesar. 1,2-PD (99.5%) and acetone (99.9%) were purchased from Sigma-Aldrich. All chemicals were used without any further purification.

Cyclic voltammetry (CV) and linear sweep voltammetry (LSV) experiments were performed in one-compartment three-electrode single-compartment cells. The glassware was stored in the acidic permanganate solution. Prior to use, the glassware was rinsed with acidic peroxide solution and MilliQ water, following by boiling for several times with MilliQ water.

A Pt wire and a home-made reversible hydrogen electrode (RHE) were used as the counter and reference electrodes, respectively. For the LSV scan with a negative potential and a corresponding large current, a dimensionally stable anode (DSA, Magneto) was used as the counter electrode instead to avoid the anode corrosion and redeposition to the working electrode.

Before each experiment, the electrolyte was purged with argon (Linde, 6.0) for at least 30 min. Electrochemical measurements were conducted on a Bio-logic VSP300 potentiostat with *iR*-correction during CV or LSV scans.

Single-Crystal Electrodes. Pt single crystals were annealed and cooled down following the protocol published by Clavilier et al [27] before electrochemical measurements. In this work, we used the three low-index surfaces (111), (100) and (110). A 3 mm bead (icryst) was used for the voltammetric experiments and a 10 mm disk (icryst) was used for the spectroscopy measurements. Before each experiment, a CV was recorded in 0.1 M H_2SO_4 solution to check that the surface was well-ordered and free from any contamination.

A Pd monolayer was electrodeposited on Pt(111) by cycling the potential between 0.9 V and 0.06 V vs. RHE in 0.1 M H_2SO_4 solution containing 10^{-4} M of $PdSO_4$ [28–30]. Because Pd deposition on Pt(110) does not show any characteristic peak, the deposition procedure was carried out in a low concentration of 2.5×10^{-6} M of $PdSO_4$ in the same potential range to better observe the evolution of the voltammetric profile [31]. The scan rate was 50 mV s^{-1}. For the Pd deposition on Pt(100) facet, it has a greater tendency to grow a second layer prior to the completion of the first one, which makes it difficult to prepare a well-defined Pd monolayer. Electrochemical nitrogen oxide (NO) annealing procedure was then adopted to improve the smoothness of the existing deposit [32]. In view of the complexity and toxicity of NO, we adopted underpotential deposition: Pd was deposited started from 0.95 V vs.RHE to negative potentials (lower limit is 0.7 V vs.RHE) in a solution containing 0.1 M H_2SO_4, 10^{-4} M $PdCl_2$, and 9×10^{-3} M HCl at very low scan rate of 0.1 mV s^{-1}, until a charge of 418 μC cm^{-2} was obtained, which corresponds to one Pd atomic layer [33]. After that, an electrochemical annealing process was conducted by cycling voltammetry of the prepared electrode between 0.4 V and 0.06 V vs.RHE at 10 mV s^{-1} in 0.1 M H_2SO_4 solution. We refer to these monolayer surfaces as $Pd_{ML}Pt(111)$, $Pd_{ML}Pt(110)$, and $Pd_{ML}Pt(100)$.

After deposition, the Pd monolayer surface was thoroughly rinsed with ultrapure water and then characterized CV in 0.1 M H_2SO_4 solution. After each experiment, Pd film was removed from the Pt substrate by immersing the electrode to a concentrated nitric acid for 2 min (bead) or 5 min (disk).

Polycrystalline Pt, Pd and gold (Au) electrodes were polished using diamond (1, 0.25, and 0.05 μm), respectively. After that, the electrodes were sonicated in MillQ water for 5 min. The electrodes were then transferred to a fresh 0.1 M H_2SO_4 solution and cycled in the range of 0.05 V – 1.55 V vs.RHE (Pt and Pd) or 0 – 1.65 V vs.RHE (Au) until a stable standard CV was obtained. Experiments were performed in hanging meniscus as for the single crystals.

***In-situ* Fourier Transformation Infrared Spectroscopy (*in-situ* FITR).** *In-situ* FTIR was performed to detect products of acetol reduction. The measurements were carried out with a Bruker Vertex 80 V IR spectrophotometer in an external reflection configuration, where the single crystals were pressed against the prismatic window and the solution species were trapped in the thin layer. A CaF_2 prism bevelled at 60° was used, and the spectra were

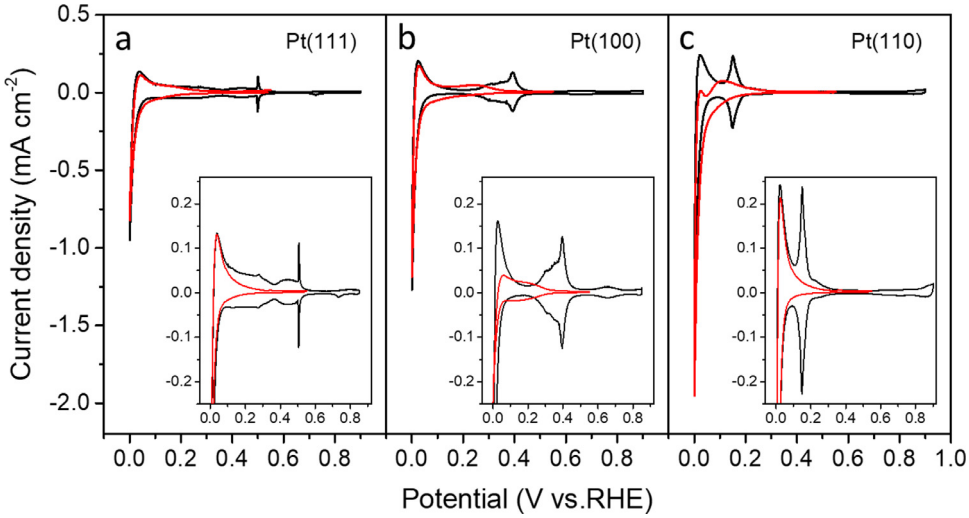

Fig. 1. CVs of different Pt surfaces (black curve) and the 1st cycle in the presence of 0.1 M acetol (red curve) in 0.1 M H_2SO_4 solution. (a) CV on Pt(111), (b) CV on Pt(100), and (c) CV on Pt(110). The inset in each panel represents CV of Pt surface (black curve) and the 20th cycle in the presence of 0.1 M acetol (red curve), which is the stable CV without any obvious changes upon further scanning. The scan rate is 50 mV s^{-1}. (For interpretation of the references to color in this figure legend, the reader is referred to the web version of this article.)

recorded at an average of 300 interferograms with 8 cm^{-1} resolution using p-polarized light.

Spectra were recorded in the range between 3000 cm^{-1} and 1100 cm^{-1}. All the spectra in this work are presented as absorbance, hence the negative bands indicate the adsorbed reactant or the consumed species, while the positive bands indicate a reorientation of the adsorbed species or the produced species [18].

Online High Performance Liquid Chromatography (HPLC). Online sampling procedure has been described elsewhere [34]. Briefly, a small Teflon tip (with an inner diameter of 0.38 mm) was placed at ca. 10 μm from the center of the electrode surface, and the other side of the tip was connected to a PEEK capillary with inner/outer diameters of 0.13/1.59 mm.

Samples with a volume of 60 μL were collected using a fraction collector (FRC-10A, Shimadzu) at the flow rate of 60 μL/min (LC-20AT pump, Shimadzu), along with the LSV at the scan rate of 1 mV s^{-1} from 0 V to -2.0 V vs.RHE. Therefore, each sample reflects the average concentration of a 60 mV potential interval.

Electrolysis at the constant potential was conducted in the H-cell divided by Nafion proton exchange membrane. Each compartment contained 7 mL of the electrolyte with 0.1 M acetol. The samples were analyzed by HPLC (LC-20A, Shimadzu) using an autosampler (SIL-20A). 20 μL of each sample was injected into the column. An Aminex HPX 87-H (Bio-Rad) column together with a Micro-Guard Cation H Cartridge (Bio-Rad) in series with a Sugar SH1011 (Shodex) column were used. The eluent was 5 mM H_2SO_4 with the flow rate of 0.6 mL min^{-1}. The column temperature was set to 85 °C for 1,2-PD separation and 45 °C for acetone separation. The separated compounds were detected with a refractive index detector (RID-10A).

3. Results and discussion

CV of acetol adsorption and reduction on single crystals. Fig. 1 shows the CV of Pt electrodes with three low-index surfaces before and after adding 0.1 M acetol in 0.1 M H_2SO_4 solution. For Pt(111), Fig. 1a (black curve), a sharp spike at about 0.5 V vs.RHE is attributed to the sulfate adlayer [35]. In the presence of acetol (red curve), we observe the entire suppression of this anion adsorption/desorption, which indicates that acetol or its derived species can adsorb strongly on the Pt(111) surface. Moreover, the inset presents the stable CV upon cycling after adding acetol, showing how the hydrogen adsorption/desorption region is suppressed increasingly. We conclude again that acetol or its decomposed species adsorbs on Pt(111) surface. As they cannot be stripped off reductively, these species might cause surface poisoning. However, the hydrogen evolution and the subsequent hydrogen oxidation are less affected by the adsorbed species, implying that the surface may not be fully covered or that the active sites for hydrogen evolution/oxidation are not entirely blocked.

On the Pt(100) surface, a broad feature due to hydrogen and anion adsorption/desorption between 0.2 and 0.45 V vs.RHE is suppressed in the presence of acetol (red curve in Fig. 1b). This also reveals the presence of adsorbed acetol or its decomposition product. From the inset in Fig. 1b, we observe a negative shift of hydrogen adsorption/desorption after continuous scans in the presence of acetol, the current density of which is a linear function of the scan rate (Figure S1), confirming that it corresponds to a surface electrochemical process. Particularly, hydrogen evolution is suppressed much more on Pt(100) than on Pt(111), also leading to only a small current for hydrogen re-oxidation. This implies that the coverage of poisoning species on the Pt(100) surface, or its occupation of the active sites for hydrogen evolution, is higher than on Pt(111).

The electrochemical reduction of acetol is more evident on the Pt(110) electrode (Fig. 1c). In the presence of acetol, the peak at 0.15 V vs. RHE corresponding to the replacement between hydrogen and hydroxyl groups is largely blocked (red curve), along with a slightly higher reduction current before going to the hydrogen evolution region in the negative-going scan. If we scan back in the positive-going direction, a tiny reduction peak at 0.05 V vs.RHE is observed, which we ascribe to acetol reduction. However, upon cycling, the cathodic wave of acetol reduction disappears and the hydrogen/hydroxyl feature is entirely blocked (inset in Fig. 1c). This implies again the poisoning of Pt(110) surface although it does not block the active sites of hydrogen evolution, similar to the situation on the Pt(111) surface.

In order to gain more insight into the poisoning species on three surfaces, we swept the CV to 0.9 V vs.RHE after adding acetol (Figure S2). All surfaces show oxidation currents between 0.7 and 0.9 V vs.RHE in the positive-going scan, which are most reasonably ascribed to CO oxidation [36]. It is not surprising that CO is the poisoning species as there have been analogous reports on acetone [37], ethanol [38] and ethyl pyruvate [39] dissociation to

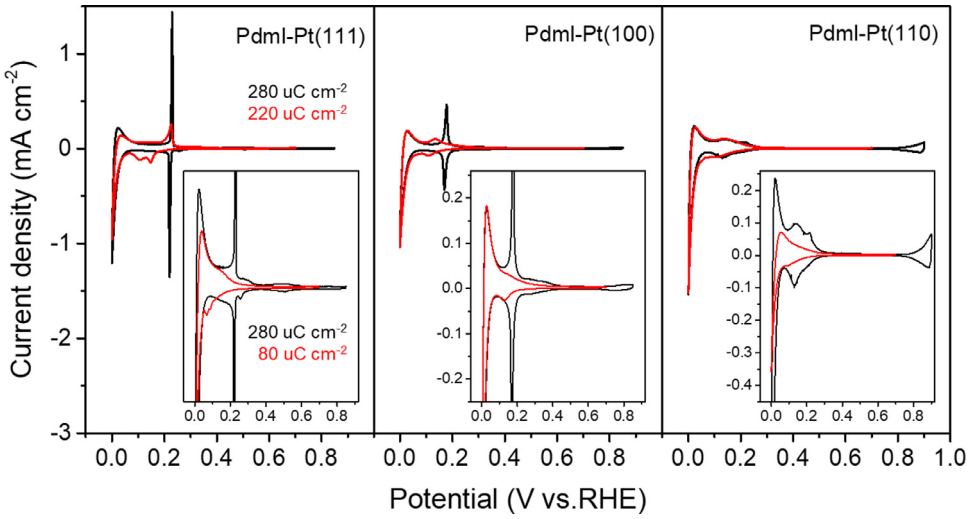

Fig. 2. CVs of bare $Pd_{ML}Pt$ surface (black curve) and the 1st cycle in the presence of 0.1 M acetol (red curve) in 0.1 M H_2SO_4 solution. (a) CV on $Pd_{ML}Pt(111)$, (b) CV on $Pd_{ML}Pt(100)$, and (c) CV on $Pd_{ML}Pt(110)$. The inset in each panel represents CV of $Pd_{ML}Pt$ surface (black curve) and the 20th cycle in the presence of 0.1 M acetol (red curve), which is the stable CV without any obvious changes upon further scanning. The scan rate is 50 mV s^{-1}. (For interpretation of the references to color in this figure legend, the reader is referred to the web version of this article.)

CO on Pt electrodes. In agreement with the above observations on the extent of poisoning, the CO stripping peak charge is higher on Pt(100) than on Pt(111) and Pt(110). The oxidation wave between 0.4 and 0.8 V vs.RHE in the negative-going scan is probably due to acetol oxidation on the non-poisoned surface. The same has also been observed for acetone reduction on Pt(100) [10].

To summarize: acetol can be reduced slowly on the Pt(110) surface in the investigated potential window, while for the other two surfaces, there is no clear reduction feature in the CV. All three surfaces suffer from poisoning to a varying degree, and Pt(100) shows the most prominent dissociative adsorption to CO.

Fig. 2 compares the CVs of the $Pd_{ML}Pt$ electrodes (black curves) with those obtained in the presence of 0.1 M acetol in 0.1 M H_2SO_4 solution (red curves). As shown in Fig. 2a, a pair of reversible sharp peaks at 0.23 V vs.RHE (positive-going scan) and 0.22 V vs.RHE (negative-going scan) indicate the replacement of adsorbed hydrogen by adsorbed (bi)sulfate and vice versa, respectively (black curve) [29,40]. After adding acetol, the original sharp peak in the negative scan is completely suppressed, and two small reduction waves arise at 0.15 V and 0.1 V vs.RHE (red curve). The charge corresponding to these two peaks (220 μC cm^{-2}) is lower than that of a full hydrogen monolayer without acetol addition (240 μC cm^{-2}). Moreover, while scanning back, the sharp peak is mostly inhibited as well, and the charges of the negative and positive waves are identical. Therefore, it is unlikely that the two reduction features belong to acetol reduction.

Upon cycling, the two reduction waves diminish, associated with the appearance of two even more tiny peaks at 0.06 V and 0.09 V vs.RHE (inset in Fig. 1a, red curve). The charge corresponding to these new peaks (80 μC cm^{-2}) represents only one third of the charge for hydrogen adsorption (240 μC cm^{-2}), indicating that the sites for hydrogen adsorption are hindered by adding acetol. There is also a lower hydrogen oxidation current compared to that in the absence of acetol.

The linear relationship of current density as function of the scan rate for the reversible peaks at ca. 0.13 V vs.RHE suggests a surface-confined process on $Pd_{ML}Pt(111)$ (Figure S3a and S3d). For the peaks at 0.06 V (negative scan) and 0.08 V (positive scan), it seems conceivable if they are assigned to the redox of the adsorbed acetol. However, as explained for acetophenone hydrogenation on Pt(111) surface [14], this redox reaction requires the cleavage and formation of C–H and O–H bond. It seems unlikely that this would lead to a reversible process. There might be other adsorbate exchange reactions on the surface of the $Pd_{ML}Pt(111)$ electrode, which we are not able to detect from CV only.

The electrochemical behavior on $Pd_{ML}Pt(100)$ is shown in Fig. 2b. In the presence of 0.1 M acetol, the reversible peaks of hydrogen/(bi)sulfate adsorption and desorption are shifted negatively by the adsorption of acetol. The linear dependence of the peak current vs. scan rate corroborates the redox process of the surface adsorbed hydrogen (Figure S3b and S3e). The inset in Fig. 2b indicates the slight poisoning of surface upon cycling, whereas the active sites for the hydrogen evolution are not affected.

On the $Pd_{ML}Pt(110)$ surface, there is barely a difference before and after adding acetol in the 1st CV scan (Fig. 2c), affirming a weak interaction between the molecule and the surface. The linear dependence of the peak current on the scan rate confirms hydrogen adsorption and desorption between 0.05 V to 0.3 V vs.RHE (Figure S3c and S3f). Different from the other two surfaces, the current at 0 V vs.RHE becomes blocked on $Pd_{ML}Pt(110)$ with continuous cycling (inset in Fig. 2c). This indicates that the surface poisoning species which originates from acetol dissociation inhibits hydrogen evolution and the subsequent re-oxidation.

The CV responses in Fig. 2 reveal that acetol adsorbs on different facets of $Pd_{ML}Pt$ electrodes weakly and with slow kinetics. $Pd_{ML}Pt(110)$ displays more severe poisoning than the other two surfaces. However, it is difficult to determine if acetol reduction takes place or not in the potential window of hydrogen adsorption.

Chronoamperometry and bulk electrolysis. In order to check whether the reduction takes place, and which products are formed, we performed bulk electrolysis at 0 V vs.RHE in 0.1 M H_2SO_4 solution containing 0.1 M acetol on the different basal planes for 2 h (the current-time transients are shown in Figure S4). However, no products were detected by HPLC on either Pt or $Pd_{ML}Pt$ single crystals. This is not surprising as all surfaces suffer from poisoning over time as observed in the CVs. It is possible that the reduction takes place on some surfaces at the beginning but the concentration is below the detection limit of HPLC.

As mentioned in the Introduction section, there are two initial reactions of acetol reduction: hydrogenation to 1,2-PD, and dehydroxylation to acetone. Thus, it could also happen that the reduced species adsorb on the surface, causing further dissociation to a surface poison before it desorbs into the solution to be detected by HPLC.

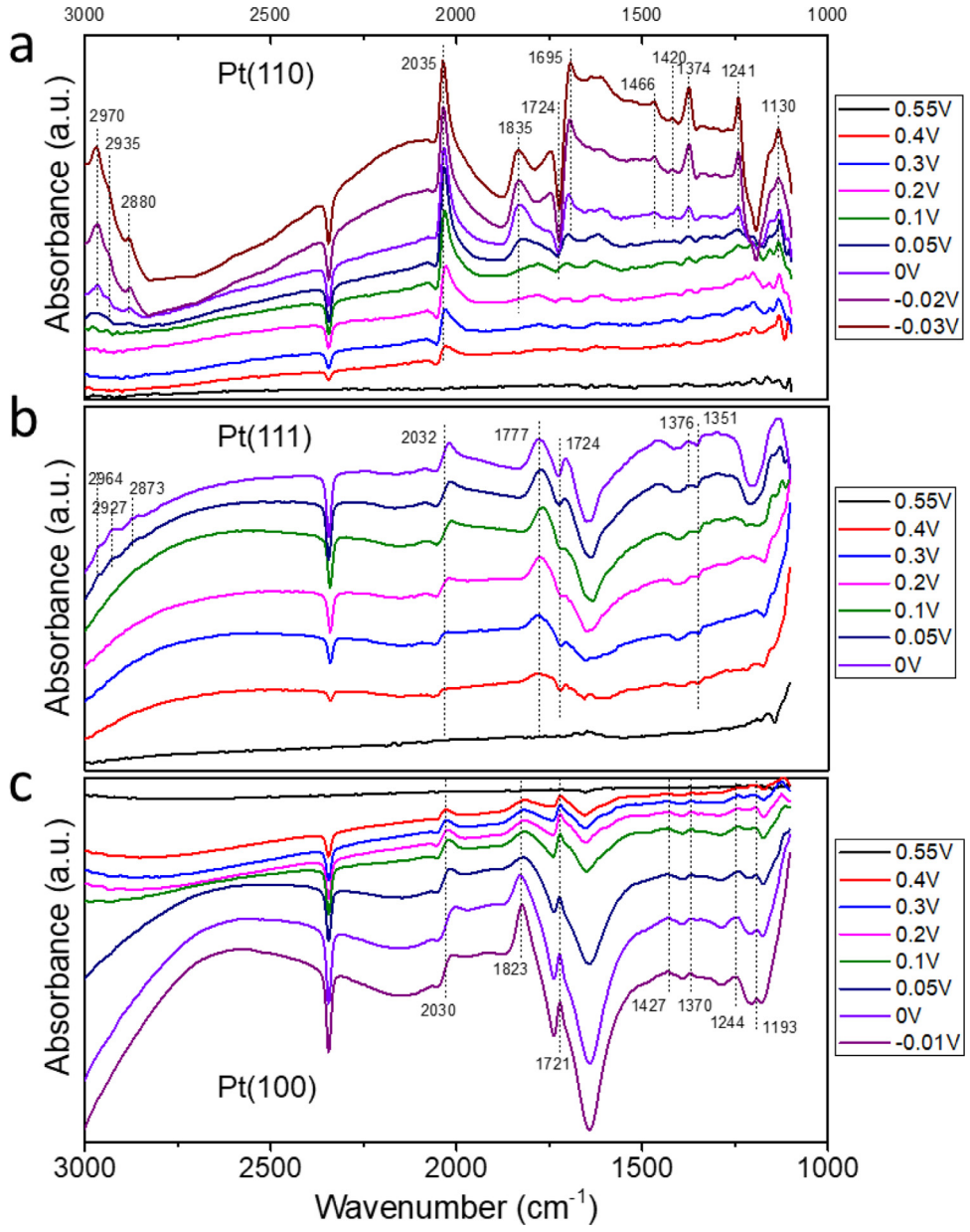

Fig. 3. *In-situ* FTIR spectra as function of potential recorded on (a) Pt(110), (b) Pt(111), and (c) Pt(100) electrodes in 0.1 M H_2SO_4 solution containing 0.1 M acetol.

The current density responses versus time on the Pt single crystals (Figure S4a) are in agreement with the CV behavior in Fig. 1. The three surfaces present attenuation in the current evolution over time, among which Pt(100) shows the lowest current density at 0 V vs.RHE, corroborating the strongest surface poisoning as observed from the CV. Bulk electrolysis on $Pd_{ML}Pt$ electrodes (Figure S4b) gives analogous responses to that obtained in Fig. 2, where the current density decreases the most on $Pd_{ML}Pt(110)$ due to the most severe poisoning on this surface.

For comparison, we also performed electrolysis in the absence of acetol at the same reaction conditions (Figure S4c-d). The current densities are higher in the blank solution than those in presence of acetol, regardless of the surface facet, which also indicates the surface poisoning during acetol reduction.

In-situ Fourier Transform Infrared Spectroscopy (In-situ FTIR). In order to gain more insight into whether acetol reduction occurs, we performed *in-situ* FTIR on all Pt and $Pd_{ML}Pt$ electrodes. P-polarized light is employed to observe the possible adsorbed intermediates or the poisoning species. Fig. 3 shows FTIR spectra recorded on the three surfaces of Pt. The reference spectrum is taken at 0.55 V vs.RHE where certainly no reduction takes place and all the other spectra are subtracted from the reference spectra.

Given that the Pt(110) facet appears to reduce acetol in the H_{UPD} region according to the CV, we first performed FTIR measurements on this surface (Fig. 3a). At a potential of 0.3 V vs.RHE, a negative band at 1724 cm^{-1} becomes visible, which is assigned to C=O stretching vibration of acetol [41,42]. This could be an indication of acetol adsorption instead of consumption since we did not observe any other positive bands that might be related to the formation of a product species at this potential. It coincides with the CV in Fig. 1c that acetol adsorbs at 0.3 V vs.RHE.

After the potential is stepped to 0 V vs.RHE and below, we observed a series of positive bands: the features at 2970, 2935, and 2880 cm^{-1} can be attributed to the symmetric and asymmetric stretching vibrations of C-H bond in 1,2-PD [43], representing

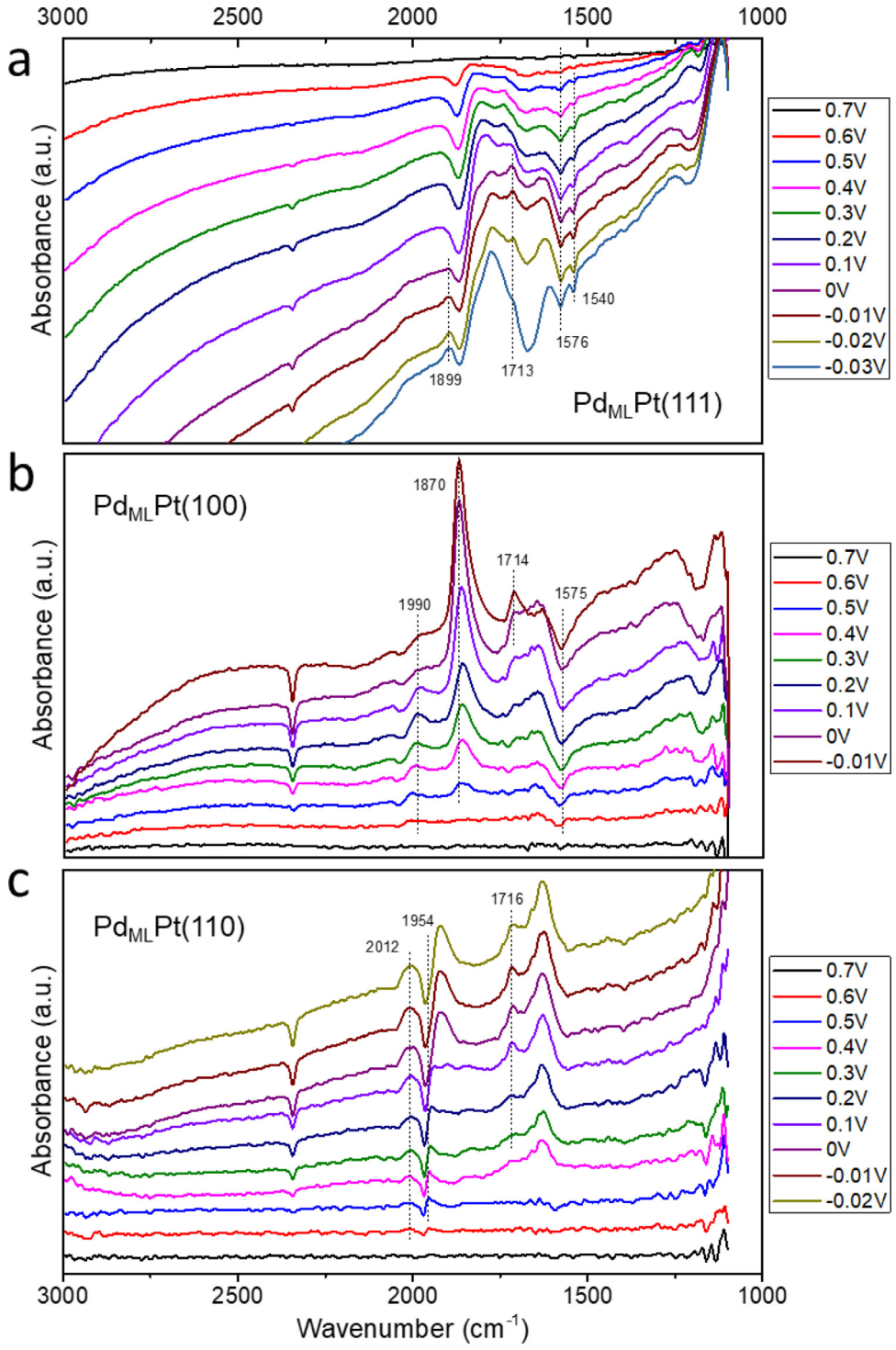

Fig. 4. *In-situ* FTIR spectra as function of potential recorded on (a) $Pd_{ML}Pt(111)$, (b) $Pd_{ML}Pt(100)$, and (c) $Pd_{ML}Pt(110)$ electrodes in 0.1 M H_2SO_4 solution containing 0.1 M acetol.

$\nu_{as}(CH_3)$ at 2970 cm^{-1}, $\nu_{as}(CH_2)$ + $\nu(CH)$ at 2935 cm^{-1}, as well as $\nu_s(CH_2)$ + $\nu_s(CH_3)$ at 2880 cm^{-1}, respectively. In addition, the other two peaks located at 1466 and 1130 cm^{-1} are assigned to CH_3 deformation and C–O stretching vibration of 1,2-PD [43], respectively.

Aside from the features corresponding to 1,2-PD, the other positive bands at 1695, 1420, 1374, and 1241 cm^{-1} can be ascribed to acetone. These bonds correspond to the symmetric carbonyl group stretching (ν_s(C=O)=1710 cm^{-1}), asymmetric CH_3 deformation ($\delta_{as}(CH_3)$=1410/1435 cm^{-1}), symmetric CH_3 deformation ($\delta_s(CH_3)$=1361 cm^{-1}), as well as asymmetric stretching of the carbon skeleton (ν_{as}(Me–C–Me)=1220 cm^{-1}) of acetone [10,44], respectively. The peak shift indicates the interaction of acetone with the solution or with the electrode surface.

On the Pt(111) surface, the negative bands at 1724 and 1351 cm^{-1} are ascribed to the carbonyl group stretching and the symmetric CH_3 bending of the adsorbed acetol, respectively (Fig. 3b), similar to the observations on Pt(110). When the poten-

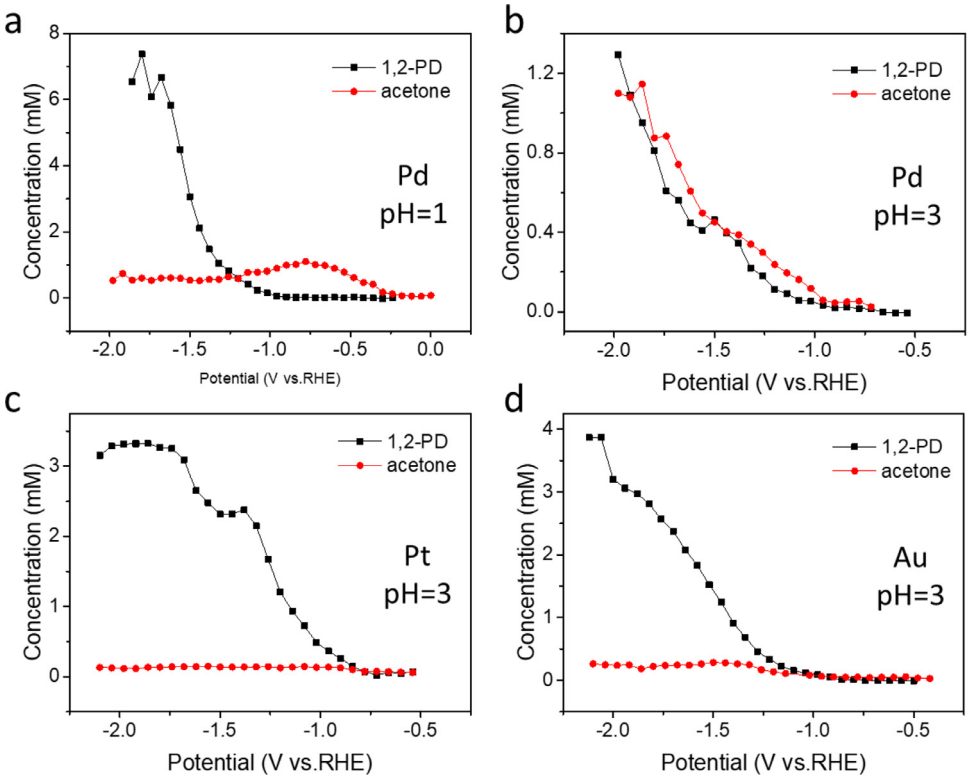

Fig. 5. Product distribution of acetol reduction (0.1 M) on (a-b) Pd, (c) Pt, and (d) Au electrodes, determined during linear sweep voltammetry from 0 to -2.2 V vs.RHE with a scan rate of 1 mV s^{-1}. pH = 1: 0.1 M H_2SO_4; pH=3: 0.001 M H_2SO_4 + 0.099 M Na_2SO_4.

tial is stepped to 0 V vs.RHE, the arising positive bands can be attributed to 1,2-PD and acetone as aforementioned. Some bands with respect to 1,2-PD and acetone are missing because of the interference by the broad band of the water layer located at around 1675 cm^{-1}.

The Pt(100) electrode shows different FTIR features compared to the other two surfaces (Fig. 3c). First of all, no specific bands assigned to 1,2-PD or acetone were observed. Secondly, a positive band at 1721 cm^{-1} becomes prominent within the applied potential window, which might be ascribed to the carbonyl group stretching of acetol [41,42]. This can be further confirmed by the positive bands at 1427 cm^{-1} (H–C–H bending in CH_3 group), 1370 cm^{-1} (symmetric CH_3 bending), 1244 cm^{-1} (C-OH bending), and 1193 cm^{-1} (C-C stretching) of acetol (see SI for the detailed explanation) [41,42].

The interpretation of these bands is ambiguous except for the conclusion that Pt(100) is inactive for acetol reduction. Enolization and aldol condensation reactions are ruled out as no extra bands other than those represented for acetol are observed. We therefore assume that acetol might desorb when the poisoned species increases its occupation on the Pt(100) surface as the potential is stepped in the negative direction. It coincides with the CV results that the Pt(100) surface suffers from the most severe poisoning. This desorption can also explain the lack of acetol reduction at around 0 V vs. RHE.

In addition to the organic species, other remarkable bands between 2100 and 1700 cm^{-1} are observed at all the three surfaces, which can be assigned to CO formation with linearly (ca. 2000 cm^{-1}) and bridge/multiple bonded (ca. 1850/1770 cm^{-1}) modes on Pt [45]. The existence of CO_2 in the atmosphere interferes with the origin of CO formation to some degree. However, CO_2 reduction (saturated CO_2 in 0.1 M H_2SO_4 solution) on the Pt electrode suggests that the onset potential for CO production is about 0.2 V vs.RHE (Figure S5). Combining the full spectra at each stepped potential in Figure S6-S8, we conclude that at least part of CO stems from dissociative adsorption of acetol, demonstrating CO being the poisoning species on each facet of the Pt electrode. This is also consistent with the CV results in Figure S2.

In conclusion, acetol can be either hydrogenated to 1,2-PD or dehydroxylated to acetone on Pt(110) and Pt(111) electrodes at the onset potential of around 0 V vs.RHE, albeit at very slow rate. In addition, acetol reduction is inhibited by poisoning of the adsorbed CO species on the Pt(100) electrode.

Next, we performed FTIR experiments on $Pd_{ML}Pt$ electrodes (Fig. 4). The reference spectrum was taken at 0.7 V vs.RHE. From the recorded spectra, no acetol reduction takes place on any surfaces, at least not in the applied potential window. A positive band at about 1715 cm^{-1} – appearing at 0 V vs.RHE for $Pd_{ML}Pt(111)$ and $Pd_{ML}Pt(100)$ surfaces and at 0.1 V vs.RHE for $Pd_{ML}Pt(110)$ – may be ascribed to enol formation of acetol according to DFT calculations [41].

Particularly, two new negative peaks at 1576 and 1540 cm^{-1} are observed on $Pd_{ML}Pt(111)$ surface (Fig. 4a), which may stem from the C=C stretching in the dimer produced by aldol condensation of acetol [41]. On $Pd_{ML}Pt(100)$ surface, a broad negative band located at 1575 cm^{-1} can be attributed to the same species (Fig. 4b). This phenomenon suggests the adsorption of a dimer species when the potential is stepped in the negative direction. On the $Pd_{ML}Pt(110)$ surface, the spectra do not show any bands ascribed to aldol condensation of acetol (Fig. 4c).

Furthermore, analogously to acetol dissociation behavior on Pt electrodes, CO poisoning species were observed in the window between 2000 and 1870 cm^{-1} on the three surfaces of $Pd_{ML}Pt$ electrodes. In order to check the stability of Pd monolayer over the course of spectra collection, we characterized CV after the FTIR experiment. Figure S9 suggests that the monolayers on the three surfaces maintain their integrity.

Online HPLC on other metal electrodes. To access practical application, we further assess the activity and selectivity of acetol reduction by extending the study on other electrodes in electrolytes of different pH and at more negative potentials, where acetol reduction is convoluted with hydrogen evolution. Fig. 5 shows the product distribution of acetol reduction on polycrystalline Pt, Pd, and Au electrodes, determined by online HPLC.

First of all, at pH = 1, we detected reduction products only on the Pd electrode (Fig. 5a and Figure S10a). Both hydrogenation and dehydroxylation reactions take place to produce significant concentrations of 1,2-PD and acetone, respectively. At potentials between 0 and -1.25 V vs.RHE, the selectivity is dominated by acetone, while applying a more negative potential steers the selectivity toward 1,2-PD. On Pt and Au electrodes, acetol reduction is very slow if not inactive at pH = 1.

At pH = 3, acetol can be reduced on all three electrodes (Fig. 5b-d and Figure S10b). As shown in Fig. 5c-d, 1,2-PD is the dominant product on both Pt and Au electrodes within the applied potential window, showing a lower onset potential on Pt (-0.75 V vs.RHE) over Au (-1.1 V vs.RHE). For the Pd electrode (Fig. 5b), both 1,2-PD and acetone are produced in equal amounts with a similar onset potential (-1.0 V vs.RHE).

4. Conclusion

In summary, we have reported the electrochemical adsorption and reduction of acetol on Pt single crystals and their corresponding epitaxial Pd monolayers. In addition, we studied the selective reduction of acetol to 1,2-PD and acetone, a conversion which would make part of the overall electrochemical upgrading of glycerol. The main conclusions are listed as below:

- On Pt(110) and (111) surfaces, acetol can be hydrogenated and dehydroxylated to 1,2-PD and acetone, respectively, at the onset potential of ca. 0 V vs.RHE, albeit with low rate. On the (100) surface, no reduction takes place.
- CO can be formed on all the three surfaces of Pt as a result of the dissociative adsorption of acetol, which poisons the surface. Pt(100) presents the most severe CO poisoning among the three facets.
- Acetol adsorption/reduction behavior is significantly different on the Pd monolayer surfaces compared to the bare Pt electrode. No reduction takes place but a keto-enol transformation is observed. Particularly, an acetol dimer is likely to be adsorbed on $Pd_{ML}Pt$(111) and (100) facets. The $Pd_{ML}Pt$(110) surface suffers from the most severe poisoning.
- The above conclusions point toward a relatively weaker adsorption of acetol on $Pd_{ML}Pt$ electrode compared to the unmodified Pt electrode.
- Online HPLC results at more negative potentials indicate that Pd is capable of reducing acetol to both 1,2-PD and acetone at pH = 1 and pH = 3; Au and Pt are appropriate candidates to reduce acetol to 1,2-PD at pH = 3.

In combination with the earlier work, the results in this work have elucidated the catalysts needed to develop cascade reactions through coupling glycerol dehydration or oxidation with successive reduction reactions to obtain value-added chemicals and fuels for the industrial requirement. In particular, glycerol oxidation to GA on Pt [46], and subsequent reduction of glyceraldehyde on Pd, yields 1,3-PD [22]. On the other hand, glycerol oxidation on Bi-modified Pt yields DHA [21], which may be subsequently reduced to acetol on Pd [22]. Pt and Au are then suitable catalysts to reduce acetol to 1,2-PD.

Credit Author Statement

Zhiqin Liang: Conceptualization, Methodology, Investigation, Writing - Original Draft

Matias Villalba: Methodology, Investigation, Writing - Review & Editing

Marc T. M. Koper: Conceptualization, Writing - Review & Editing, Supervision, Funding acquisition

Declaration of Competing Interest

The authors declare that they have no known competing financial interests or personal relationships that could have appeared to influence the work reported in this paper.

Acknowledgments

This research received funding from the Netherlands Organization for Scientific Research (NWO) in the framework of the fund New Chemical Innovations, project 731.015.204 ELECTROGAS, with financial support of Akzo Nobel Chemicals, Shell Global Solutions, Magneto Special Anodes (an Evoqua Brand) and Elson Technologies.

Supplementary materials

Supplementary material associated with this article can be found, in the online version, at doi:10.1016/j.electacta.2021.138911.

References

[1] C. Smith, J.H. Utley, M. Petrescu, H. Viertler, Biomass electrochemistry: anodic oxidation of an organo-solv lignin in the presence of nitroaromatics, JApEl 19 (4) (1989) 535–539.
[2] LiChum, H.; Baizer, M. M. The electrochemistry of biomass and derived materials. 1985.
[3] Y. Feng, L. Tao, Z. Zheng, H. Huang, F. Lin, Upgrading agricultural biomass for sustainable energy storage: Bioprocessing, electrochemistry, mechanism, Energy Storage Mater. 31 (2020) 274–309.
[4] H. Yang, R. Yan, H. Chen, D.H. Lee, C. Zheng, Characteristics of hemicellulose, cellulose and lignin pyrolysis, Fuel 86 (12-13) (2007) 1781–1788.
[5] P. Tanger, J.L. Field, C.E. Jahn, M.W. DeFoort, J.E. Leach, Biomass for thermochemical conversion: targets and challenges, Front. Plant Sci. 4 (2013) 218.
[6] Y. Kwon, Y.Y. Birdja, S. Raoufmoghaddam, M.T.M Koper, Electrocatalytic hydrogenation of 5-hydroxymethylfurfural in acidic solution, Chem. Sus. Chem. 8 (10) (2015) 1745–1751.
[7] Y. Kwon, M.T.M. Koper, Electrocatalytic hydrogenation and deoxygenation of glucose on solid metal electrodes, Chem. Sus. Chem. 6 (3) (2013) 455–462.
[8] S. Guan, O. Donovan-Sheppard, C. Reece, D.J. Willock, A.J. Wain, G.A. Attard, Structure sensitivity in catalytic hydrogenation at platinum surfaces measured by shell-isolated nanoparticle enhanced Raman spectroscopy (SHINERS), ACS Catal. 6 (3) (2016) 1822–1832.
[9] F. Delbecq, P. Sautet, Competitive C=C and C=O Adsorption of α-β-Unsaturated Aldehydes on Pt and Pd surfaces in relation with the selectivity of hydrogenation reactions: a theoretical approach, J. Catal. 152 (2) (1995) 217–236.
[10] C.J. Bondue, F. Calle-Vallejo, M.C. Figueiredo, M.T. Koper, Structural principles to steer the selectivity of the electrocatalytic reduction of aliphatic ketones on platinum, Nat. Catal. 2 (3) (2019) 243–250.
[11] T. Hartung, H. Baltruschat, Differential electrochemical mass spectrometry using smooth electrodes: adsorption and hydrogen/deuterium exchange reactions of benzene on platinum, Langmuir 6 (5) (1990) 953–957.
[12] M.P. Soriaga, A.T. Hubbard, Determination of the orientation of adsorbed molecules at solid-liquid interfaces by thin-layer electrochemistry: aromatic compounds at platinum electrodes, J. Am. Chem. Soc. 104 (10) (1982) 2735–2742.
[13] A. Shayeghi, S. Krähling, P. Hörtz, R. Johnston, C. Heard, R. Schäfer, Adsorption of acetonitrile, benzene, and benzonitrile on Pt (111): single crystal adsorption calorimetry and density functional theory, J. Phys. Chem. C. 121 (39) (2017) 21354–21363.
[14] C.J. Bondue, M.T. Koper, Electrochemical reduction of the carbonyl functional group: the importance of adsorption geometry, molecular structure, and electrode surface structure, J. Am. Chem. Soc. 141 (30) (2019) 12071–12078.
[15] S.J. Cleghorn, D. Pletcher, The mechanism of electrocatalytic hydrogenation of organic molecules at palladium black cathodes, Electrochim. Acta 38 (2-3) (1993) 425–430.

[16] R.S. Sherbo, A. Kurimoto, C.M. Brown, C.P. Berlinguette, Efficient electrocatalytic hydrogenation with a palladium membrane reactor, J. Am. Chem. Soc. 141 (19) (2019) 7815–7821.
[17] X. Chen, M.T. Koper, Mass-transport-limited oxidation of formic acid on a PdMLPt (100) electrode in perchloric acid, Electrochem. Commun. 82 (2017) 155–158.
[18] M.A. Villalba, M.T. Koper, Structure sensitivity of acetophenone reduction on palladium-modified platinum single-crystal electrodes, J. Phys. Chem. C. 124 (47) (2020) 25884–25891.
[19] A.C. Garcia, M.J. Kolb, C. van Nierop y Sanchez, J. Vos, Y.Y. Birdja, Y. Kwon, G. Tremiliosi-Filho, M.T. Koper, Strong impact of platinum surface structure on primary and secondary alcohol oxidation during electro-oxidation of glycerol, ACS Catal. 6 (7) (2016) 4491–4500.
[20] A.C. Garcia, Y.Y. Birdja, G. Tremiliosi-Filho, M.T. Koper, Glycerol electro-oxidation on bismuth-modified platinum single crystals, J. Catal. 346 (2017) 117–124.
[21] Y. Kwon, Y. Birdja, I. Spanos, P. Rodriguez, M.T. Koper, Highly selective electro-oxidation of glycerol to dihydroxyacetone on platinum in the presence of bismuth, ACS Catal. 2 (5) (2012) 759–764.
[22] Z. Liang, M.A. Villalba, G. Marcandalli, K. Ojha, A.J. Shih, M.T. Koper, Electrochemical reduction of the simplest monosaccharides: dihydroxyacetone and glyceraldehyde, ACS Catal. 10 (23) (2020) 13895–13903.
[23] M. Stratmann, Volume 8, Organic Electrochemistry; Schäfer, HJ, Ed., Wiley-VCH Weinheim, 2004.
[24] C.W. Chiu, M.A. Dasari, G.J. Suppes, W.R. Sutterlin, Dehydration of glycerol to acetol via catalytic reactive distillation, AIChE 52 (10) (2006) 3543–3548.
[25] M.H. Mohamad, R. Awang, W.M. Yunus, A review of acetol: application and production, Am. J. Appl. Sci. 8 (11) (2011) 1135.
[26] W. Sauter, O.L. Bergmann, U. Schröder, Hydroxyacetone: a glycerol-based platform for electrocatalytic hydrogenation and hydrodeoxygenation processes, Chem. Sus. Chem. 10 (15) (2017) 3105–3110.
[27] J. Clavilier, D. Armand, S. Sun, M. Petit, Electrochemical adsorption behaviour of platinum stepped surfaces in sulphuric acid solutions, J. Electroanal. Chem. Interf. Electrochem. 205 (1-2) (1986) 267–277.
[28] J. Inukai, M. Ito, Electrodeposition processes of palladium and rhodium monolayers on Pt (111) and Pt (100) electrodes studied by IR reflection absorption spectroscopy, J. Electroanal. Chem. 358 (1-2) (1993) 307–315.
[29] M. Llorca, J. Feliu, A. Aldaz, J. Clavilier, Electrochemical structure-sensitive behaviour of irreversibly adsorbed palladium on Pt (100), Pt (111) and Pt (110) in an acidic medium, J. Electroanal. Chem. 351 (1-2) (1993) 299–319.
[30] G.A. Attard, A. Bannister, The electrochemical behaviour of irreversibly adsorbed palladium on Pt (111) in acid media, J. Electroanal. Chem. Interf. Electrochem. 300 (1-2) (1991) 467–485.
[31] J. Souza-Garcia, A. Berná, E. Ticianelli, V. Climent, J. Feliu, Electrochemical properties of palladium adlayers on Pt (110) substrates, J. Electroanal. Chem. 660 (2) (2011) 276–284.
[32] B. Alvarez, A. Berna, A. Rodes, J. Feliu, Electrochemical properties of palladium adlayers on Pt (1 0 0) substrates, Surf. Sci. 573 (1) (2004) 32–46.
[33] B.A. Previdello, E. Sibert, M. Maret, Y. Soldo-Olivier, Palladium Electrodeposition onto Pt (100): Two-Layer Underpotential Deposition, Langmuir 33 (9) (2017) 2087–2095.
[34] Y. Kwon, M.T. Koper, Combining voltammetry with HPLC: application to electro-oxidation of glycerol, AnaCh 82 (13) (2010) 5420–5424.
[35] A. Funtikov, U. Stimming, R. Vogel, Anion adsorption from sulfuric acid solutions on Pt (111) single crystal electrodes, J. Electroanal. Chem. 428 (1-2) (1997) 147–153.
[36] N. Lebedeva, M. Koper, E. Herrero, J. Feliu, R. Van Santen, Cooxidation on stepped Pt [n (111)×(111)] electrodes, J. Electroanal. Chem. 487 (1) (2000) 37–44.
[37] C.J. Bondue, Z. Liang, M.T. Koper, Dissociative adsorption of acetone on platinum single-crystal electrodes, J. Phys. Chem. C. (2021).
[38] S.C. Lai, S.E. Kleyn, V. Rosca, M.T. Koper, Mechanism of the dissociation and electrooxidation of ethanol and acetaldehyde on platinum as studied by SERS, J. Phys. Chem. C. 112 (48) (2008) 19080–19087.
[39] O.A. Hazzazi, S.E. Huxter, R. Taylor, B. Palmer, L. Gilbert, G.A. Attard, Electrochemical studies of irreversibly adsorbed ethyl pyruvate on Pt {h k l} and epitaxial Pd/Pt {h k l} adlayers, J. Electroanal. Chem. 640 (1-2) (2010) 8–16.
[40] X. Chen, L.P. Granda-Marulanda, I.T. McCrum, M.T. Koper, Adsorption processes on a Pd monolayer-modified Pt (111) electrode, Chem. Sci. 11 (6) (2020) 1703–1713.
[41] K. Koichumanova, A.K.K. Vikla, R. Cortese, F. Ferrante, K. Seshan, D. Duca, L. Lefferts, In situ ATR-IR studies in aqueous phase reforming of hydroxyacetone on Pt/ZrO2 and Pt/AlO (OH) catalysts: the role of aldol condensation, Appl. Catal. B 232 (2018) 454–463.
[42] V. Mohaček-Grošev, Vibrational analysis of hydroxyacetone, Spectrochim. Acta A 61 (3) (2005) 477–484.
[43] C.R. Ayre, R.J. Madix, The adsorption and reaction of 1, 2-propanediol on Ag (110) under oxygen lean conditions, Surf. Sci. 303 (3) (1994) 279–296.
[44] N.R. Avery, EELS identification of the adsorbed species from acetone adsorption on Pt (111), Surf. Sci. 125 (3) (1983) 771–786.
[45] K. Kunimatsu, T. Sato, H. Uchida, M. Watanabe, Role of terrace/step edge sites in CO adsorption/oxidation on a polycrystalline Pt electrode studied by in situ ATR-FTIR method, Electrochim. Acta 53 (21) (2008) 6104–6110.
[46] Y. Kwon, K.J.P. Schouten, M.T. Koper, Mechanism of the catalytic oxidation of glycerol on polycrystalline gold and platinum electrodes, Chem. Cat. Chem. 3 (7) (2011) 1176–1185.